The Journal of Chemical Physics ARTICLE pubs.aip.org/aip/jcp

Models to predict configurational adiabats of Lennard-Jones fluids and their transport coefficients

Cite as: J. Chem. Phys. 161, 084502 (2024); doi: 10.1063/5.0225650
Submitted: 26 June 2024 • Accepted: 8 August 2024 •
Published Online: 28 August 2024

D. M. Heyes,[1,a] D. Dini,[1] S. Pieprzyk,[2] A. C. Brańka,[2] and L. Costigliola[1,3]

AFFILIATIONS

[1] Department of Mechanical Engineering, Imperial College London, Exhibition Road, South Kensington, London SW7 2AZ, United Kingdom
[2] Institute of Molecular Physics, Polish Academy of Sciences, M. Smoluchowskiego 17, 60-179 Poznań, Poland
[3] Glass and Time, IMFUFA, Department of Science and Environment, Roskilde University, P.O. Box 260, DK-4000 Roskilde, Denmark

[a] **Author to whom correspondence should be addressed:** d.heyes@imperial.ac.uk

ABSTRACT

A comparison is made between three simple approximate formulas for the configurational adiabat (i.e., constant excess entropy, s_{ex}) lines in a Lennard-Jones (LJ) fluid, one of which is an analytic formula based on a harmonic approximation, which was derived by Heyes *et al.* [J. Chem. Phys. **159**, 224504 (2023)] (analytic isomorph line, AIL). Another is where the density is normalized by the freezing density at that temperature (freezing isomorph line, FIL). It is found that the AIL formula and the average of the freezing density and the melting density ("FMIL") are configurational adiabats at all densities essentially down to the liquid–vapor binodal. The FIL approximation departs from a configurational adiabat in the vicinity of the liquid–vapor binodal close to the freezing line. The self-diffusion coefficient, D, shear viscosity, η_s, and thermal conductivity, λ, in macroscopic reduced units are essentially constant along the AIL and FMIL at all fluid densities and temperatures, but departures from this trend are found along the FIL at high liquid state densities near the liquid–vapor binodal. This supports growing evidence that for simple model systems with no or few internal degrees of freedom, isodynes are lines of constant excess entropy. It is shown that for the LJ fluid, η_s and D can be predicted accurately by an essentially analytic procedure from the high temperature limiting inverse power fluid values (apart from at very low densities), and this is demonstrated quite well also for the experimental argon viscosity.

I. INTRODUCTION

The excess entropy, s_{ex}, of a system is the difference between the total entropy from what would be the ideal gas value at the same temperature and density and can be defined at all points on a fluid phase diagram. A line of constant s_{ex} on a phase diagram is called a "configurational adiabat." Each fluid state point falls on one of the many configurational adiabats, which cover the entire fluid phase.

In Ref. 1, Rosenfeld showed strong evidence that s_{ex} is a predictor for the dynamics of simple systems and he formulated the so-called excess entropy scaling of transport coefficients. This observation can be rationalized in the high density region of the phase diagram by the isomorph theory. An "isomorph" is a configurational adiabat (CA) where the correlation coefficient, R, between the virial and potential energy is close to unity (typically $R > 0.9$ is taken).[2] This condition is satisfied for fluids that are not too far from the freezing line but breaks down progressively at densities near the critical density and for lower values. Along an isomorph, a property expressed in "isomorph" or macroscopic (MU) reduced units has (to a good approximation) a constant value.[2] Some properties may satisfy this behavior, while others may not, along the same line. The invariance of structure when density scaled, for example, the radial distribution function and percolation threshold distance,[3] is a key signature of an isomorph.[2,4–7]

Only the hard sphere and inverse power potential (i.e., $\sim r^{-n}$, where r is the pair separation and $n > 3$ is the potential steepness exponent) (IPL) fluids form perfect isomorphs, and this condition is only approximately satisfied for other types of model and experimental system. An isomorph is a configurational adiabat, but a configurational adiabat is not necessarily an isomorph. There are also so-called "isodynes" where there is a MU collapse of the transport coefficients and some other dynamical properties, but not of the structure. An example of this has recently been reported for a model low temperature ionic liquid.[8,9] In fact, the current evidence is that isodynes are probably more common than isomorphs in real chemical liquid systems which have many internal degrees of freedom.[9]

The isomorph–isodyne treatment may be considered to be a "top down" thermodynamic-based theoretical approach, as the specific nature of the molecular level structural evolution and dynamics is not considered. While there are many "bottom up" theories of liquids in the literature, which start from a molecular level foundation, they require approximations when the molecular level many-body processes need to be included in the theory. Both approaches are complementary, and combined can be used to quantify dynamical and transport processes in liquids, which discriminate between different chemical systems. Unlike the van der Waals equation of state scaling, which uses constants based on the interaction pair potential to collapse the data, the MU scaling is carried out with state point dependent parameters that are independent of the pair potential.

The Lennard-Jones (LJ) pair potential has been widely used to represent generically some of the important aspects of the interaction between small molecules. The LJ expression is composed of a repulsive r^{-12} and an attractive r^{-6} IPL term, $\phi(r) = 4\varepsilon[(\sigma/r)^{12} - (\sigma/r)^{6}]$, where ε and σ set the interparticle energy and length scales, respectively. The shear viscosity, η_s, self-diffusion coefficient, D, and thermal conductivity, λ, of the LJ fluid not too far from the freezing line show good MU isomorph collapse, while the bulk viscosity, η_b, does not.[3] This may be attributed in part to the fact that while the LJ structure is essentially invariant when density-scaled along the isomorph, the relative contributions to the thermodynamic properties from the two parts of the potential scale differently with density, and η_b is defined in terms of the system's total pressure fluctuations, which do not exhibit isomorphic collapse. In general, quantities that are obtained from the free energy as volume derivatives are not expected to be isomorph invariant.

In Ref. 10 (referred to as P1 herein), the isomorph MU scaling of the LJ shear viscosity, self-diffusion coefficient, and thermal conductivity was investigated. In addition, the isomorph collapse of the radial distribution function and its various derivatives were covered. This was followed in Ref. 11 (referred to as P2) by an investigation of simple analytic formulas for the CA lines, mainly based around forces and a harmonic model. The ability of liquid state perturbation theory to account for the variation in thermodynamic properties in the high temperature CA limit at reasonably high densities was demonstrated in P2.

In the present work, the behavior of the freezing density scaling discussed in P1 and the simple analytic form for a CA based on a harmonic model of the liquid of P2 are investigated further. A more accurate variant of freezing density scaling in the liquid part of the fluid phase diagram is proposed and verified using molecular dynamics (MD) simulation data of the excess entropy and transport coefficients.

One of the main themes of this work is to determine lines of constant excess entropy of the LJ fluid and to explore the behavior of key transport coefficients along these lines. It is also shown that the high temperature (i.e., IPL) limit of the CA can be used to predict the LJ transport coefficients from relatively simple parameterized expressions.

Section II presents various approximate formulas for the configurational adiabat and isomorph lines, which for the LJ system are completely analytic. A new variant of the fluid–solid coexistence density scaling approach is proposed. The harmonic model invented in P2 is used to predict s_{ex} of an arbitrary LJ fluid state point. Section III shows the excess entropy derived from MD simulations along some predicted CA lines at temperatures below $T = 2.0$, which includes the liquid–vapor domain and the lower part of the supercritical region. Section IV investigates how two of the LJ transport coefficients vary along the configurational adiabat lines, and the shear viscosity data for experimental argon are analyzed using the same procedure. Conclusions from this work are made in Sec. V.

Section II discusses a series of expressions that could be used to represent configurational adiabats of the LJ fluid.

II. ANALYTIC EXPRESSIONS FOR THE CONFIGURATIONAL ADIABAT LINES

First, as a point of definition, the inverse power potential with exponent, $n = 12$, $\phi_{ipl4} = 4\varepsilon(\sigma/r)^{12}$, used in this work is referred to as "IPL4" to make it clear that the factor of 4 is present in its definition, which is inherited from the definition of the LJ potential. IPL4 has often been used in perturbation theories of the LJ system, notably by Hansen,[12] which was based on the partition function expansion procedure of Zwanzig.[13] This perturbation theory was employed by the present authors in P2 to explain the high temperature limiting behavior of the LJ fluid along any of its configurational adiabats.

Analytic expressions of lines on the temperature–density plane that satisfy for fluids the s_{ex} = const. condition are proposed and investigated in this section. LJ units of ε for energy, σ for length and the particle mass, and m for mass are used throughout this work [e.g., time, t, is in units of $\sigma(m/\varepsilon)^{1/2}$], apart from where the quantities are further nondimensionalized into MU.

A. Coexisting fluid–solid density based models

It was shown by Khrapak and Khrapak that the transport coefficients of a range of model and experimental fluid systems expressed in MU units collapse very well as a function of ρ/ρ_{fr}, the ratio of the number density divided by the (temperature dependent) freezing density, ρ_{fr},[14–18] which was also confirmed by the present authors in P1. The ratio ρ/ρ_{fr} provides a convenient procedure to compare the behavior of fluid systems at different temperatures and could be viewed as a surrogate for the excess entropy. This procedure is referred to as Freezing Density Scaling (FDS). A list of the acronyms used in this work is given in Table I in the Appendix. This simple procedure scales out the effects of temperature for a number of LJ transport properties to a very good approximation, meaning that the

density dependence of the transport coefficients becomes essentially a line rather than a two-dimensional surface of values.[10,11]

Within this approximation, an isomorph line passing through the fluid state point, T_0, ρ_0, is "parallel" to the freezing line. The freezing isomorph line ("FIL") is defined as follows. If $\rho_{fr}(T)$ is the density of the fluid along the freezing line,

$$R_{fr} = \frac{\rho_0}{\rho_{fr}(T_0)}, \quad \rho_{FIL}(T) = R_{fr}\rho_{fr}(T), \tag{1}$$

where R_{fr} is the ratio of the reference density, ρ_0, in the fluid region of the phase diagram divided by the density along the freezing line at the same temperature (i.e., $T = T_0$). There is an accurate fitted analytic formula for the LJ freezing line, $\rho_{fr}(T)$,[19,20] which can be used, making the FIL analytic in practice.

Equation (1) implies that the freezing line is a single isomorph from the triple point to infinitely high temperature for the LJ system. It is known, however, that this is not the case, and corrections have to be made in the liquid part of the phase diagram and at slightly higher temperatures.[21–23] This suggests that freezing density scaling using the FIL formula of Eq. (1) may not give accurate configurational adiabats and isomorphs in the liquid region.

Two variants of Eq. (1) are considered in this work using different aspects of fluid–solid coexistence. These employ the melting line ("MIL"), which is at higher density, and the average of these two ("FMIL"). If $\rho_m(T)$ is the density along the melting line, the corresponding formulas for these two lines are

$$\begin{aligned} R_m &= \frac{\rho_0}{\rho_m(T_0)}, \quad \rho_{MIL}(T) = R_m\rho_m(T), \\ R_{frm} &= \frac{\rho_0}{\rho_{frm}(T_0)}, \quad \rho_{FMIL}(T) = R_{frm}\rho_{frm}(T), \end{aligned} \tag{2}$$

where $\rho_{frm}(T) = [\rho_{fr}(T) + \rho_m(T)]/2$. The $\rho_{FIL}(T), \rho_{MIL}(T)$, and $\rho_{FMIL}(T)$ lines are generically denoted by the ratio, ρ/ρ_{fm}.

The FMIL formula is an arithmetic mean of the freezing and melting densities and is therefore a hypothetical state point in the metastable solid–fluid coexistence region, which is in the same tradition as the law of rectilinear diameters for liquid–vapor coexistence. Despite the fact that the symmetries of the fluid and solid phases are different, it has been speculated that in some systems, the fluid–solid transition may manifest a critical point.[24] Consequently, the arithmetic mean of the freezing and melting densities seems an obvious first choice for such a hybrid case.

An alternative choice for a configurational adiabat line that does not depend on knowledge of the fluid–solid coexistence lines is described next.

B. Harmonic model

Rosenfeld pioneered a theoretical construction that expressed the thermodynamic and transport properties of the LJ system and even the freezing and melting transition in terms of the sum of two contributions, one derived from the r^{-12} part of the potential and the other from the attractive part, r^{-6},[1,25–27] with importantly no "cross" term, which simplifies the analytic formulation immensely. Rosenfeld proposed that for the freezing and melting curves, $T = \alpha_{12}\rho^4 - \alpha_6\rho^2$, where α_6 and α_{12} are positive constants,[25] which was subsequently employed by Khrapak *et al.*[28]

This feature is prominent in isomorph theory and was employed in P2 where a simple mean field harmonic model for a LJ isomorph line was developed, which only requires calculating the repulsive and attractive components of the potential energy at a single state point to parameterize it. This approach is an approximation to a rigorous formula involving the heat capacities of the repulsive and attractive parts of the potential,[5,15,29,30] but, nevertheless, leads to a formula with the same generic analytic form as the exact treatment. Let $\overline{T} = T/T_0$, $\overline{\rho} = \rho/\rho_0$, and $u = u_r + u_a$ be the total potential energy per particle, where u_r and u_a are the repulsive and attractive parts, respectively. Then,

$$\overline{T} = A\overline{\rho}^4 - B\overline{\rho}^2, \quad A = \frac{132u_{r,0}}{132u_{r,0} + 30u_{a,0}}, \quad B = -\frac{30u_{a,0}}{132u_{r,0} + 30u_{a,0}}, \tag{3}$$

where $u_{r,0}$ and $u_{a,0}$ are the average repulsive (r^{-12}) and attractive (r^{-6}) parts of the LJ potential energy per particle at a reference state point, ρ_0, T_0. Note that $A - B = 1$ and the value of A depends on the two variables, ρ_0 and T_0. It was shown in P2 that a single value of these two quantities gives a good representation of a complete isomorph, providing that the reference temperature is chosen at an appropriate intermediate temperature, typically along an isotherm a little above the critical point value. Then, the reference state point is in the transition regime from liquid-like to supercritical IPL dominated qualitative behavior. This was based on a few isomorphs, and a more comprehensive investigation of these preliminary results is made here.

The expression in Eq. (3) is here referred to as the analytic isomorph line (AIL).

C. Determining the *A* parameter

The A parameter in Eq. (3) depends on the repulsive and attractive parts of the potential energy per particle at the reference state point, ρ_0, T_0, which can be determined directly by MD or from a parameterized equation of state (PEOS) of the excess (i.e., configurational) part of the pressure P_{ex} using the formula $P_{ex} = \rho(4u_r + 2u_a)$. This leads to $u_r = P_{ex}/2\rho - u$ and $u_a = 2u - P_{ex}/2\rho$, as $u = u_r + u_a$ (both u and P_{ex} can be obtained directly from the PEOS). The modified Benedict–Webb–Rubin (MBWR) analytic equation of state,[32] with the parameters applicable to the LJ fluid region given in Ref. 31, was used in the present study.

Figure 1 shows the A parameter as a function of ρ_0 for three representative values of T_0 using the LJ PEOS from Refs. 31 and 33. For $T_0 = 2$, the values obtained directly by MD are also shown. The MD simulations were conducted with the Verlet leapfrog algorithm,[34] using velocity scaling,[35] and the Nosé–Hoover thermostat to control the temperature.[36]

As a precursor to the following analysis, it is convenient to parameterize $A(\rho_0, T_0)$ in terms of a low order polynomial in ρ_0 for a fixed value of T_0. MD LJ simulations were conducted at a series of densities, ρ_0, along an isotherm, and A was determined from the potential energy components using the second line expression in Eq. (3). A least squares fit to the $A(\rho_0, T_0)$ values for $T_0 = 2$ was made using the function

$$A(\rho_0, T_0) = a_0 + b_0\rho_0 + c_0\rho_0^2 + d_0\rho_0^3, \tag{4}$$

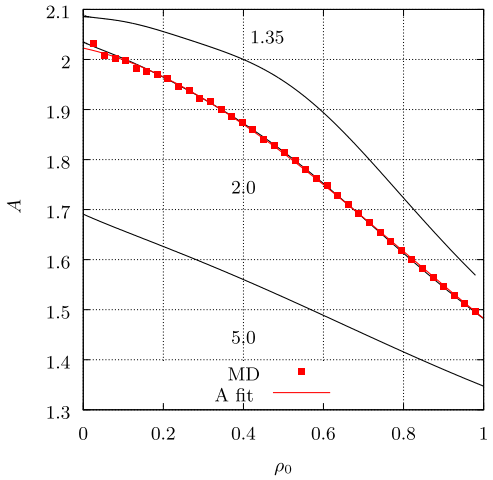

FIG. 1. The dependence of the A parameter defined in Eq. (3) as a function of ρ_0 along several isotherms, $T_0 = 1.35, 2.0$, and 5.0 calculated using the LJ PEOS as described in the main text, which are shown as continuous lines. The symbols are derived by carrying out MD simulations along the chosen isotherm and using the definition of A in terms of Eq. (3), which requires the MD-determined, $u_{r,0}$ and $u_{a,0}$.[31] The fit formula in Eq. (4) is indicated by "A fit" in the figure.

where a_0, b_0, c_0, and d_0 are 2.022 63, −0.171 304, −0.627 794, and 0.259 057, respectively. Figure 1 shows that the fit formula in Eq. (4) cannot be distinguished from the corresponding PEOS line. The A parameter is seen to be greater than unity in Fig. 1 and $A \to 1$ in the high temperature limit. In the $\rho_0 \to 0$ limit, $A = 2.09, 2.04$, and 1.69 for $T_0 = 1.35, 2.0$, and 5.0, respectively. These constants depend on T_0, and $T_0 = 2$ was used for the rest of this work. In the high temperature (density) limit along a configurational adiabat, the system tends to that of the IPL4 potential,

$$\frac{T}{T_0} = A\left(\frac{\rho}{\rho_0}\right)^4, \tag{5}$$

which gives $\rho = A^{-1/4}\rho_0$ when $T = T_0$. As $A \geq 1$, the high temperature limiting IPL crosses the T_0 line at a lower density than that of the LJ isomorph itself (i.e., ρ_0). The LJ line is

$$\frac{T}{T_0} = A\left(\frac{\rho}{\rho_0}\right)^4 + (1-A)\left(\frac{\rho}{\rho_0}\right)^2. \tag{6}$$

Equation (6) is of a form found in the literature, where in the isomorph region the parameter A is replaced by $\gamma_0/2 - 1$ and γ_0 is the so-called density-scaling exponent at a reference density and temperature.[5,37] Hence, from Eq. (6), the temperature dependence of ρ is

$$\overline{\rho}^2 = \frac{(A-1) + \sqrt{(1-A)^2 + 4A\overline{T}}}{2A}, \tag{7}$$

and $A \to 1$ in the $T_0 \to \infty$ limit as then $|u_{a,0}/u_{r,0}| \to 0$. In that limit, the expression in Eq. (7) reduces to $\overline{\rho}^4/\overline{T} = 1$, which defines the IPL4 density–temperature relationship. The density–temperature line defined through Eq. (7) is referred to as $\rho_{AIL} = \overline{\rho}\rho_0$.

Figure 2 compares the FIL, MIL, FMIL, and AIL, each of which passes through eight reference state points, ρ_0, T_0, where $T_0 = 2$ in each case. The lines terminate on the vapor or liquid part of the vapor–liquid binodal. Above about the critical temperature on the scale of Fig. 2, there is hardly any difference between the proposed isomorph lines of AIL, FIL, MIL, and FMIL, but there are noticeable differences in the liquid part of the phase diagram. Figure 2 shows that the FILs terminate on the binodal at a lower density than those of AIL, while the MILs have the highest density. The FMIL and AIL are hardly distinguishable in Fig. 2 at any density and temperature.

Figure 2 also shows that the differences between the four types of curve decrease as ρ_0 decreases, and they tend to a vertical line (i.e., an isochore) on the scale of Fig. 2 in the low reference density ρ_0 region in the $\rho_0 \to 0$ limit for $T < T_0$. Even in this low ρ_0 limit, these curves will bend over to the right in the high temperature IPL4 limit for $T \gg T_0$.

This $T < T_0$ behavior in the low density limit may be rationalized as follows. In the limit, $\rho_0 \to 0$, for $T_0 = 2$, $A \simeq 2.0$, and $B \to 1$, when Eqs. (6) and (7) become

$$\overline{T} \simeq 2\overline{\rho}^4 - \overline{\rho}^2, \quad \rho(\overline{T}) \simeq \rho_0\left(\frac{1+\sqrt{1+8\overline{T}}}{4}\right)^{1/2}, \tag{8}$$

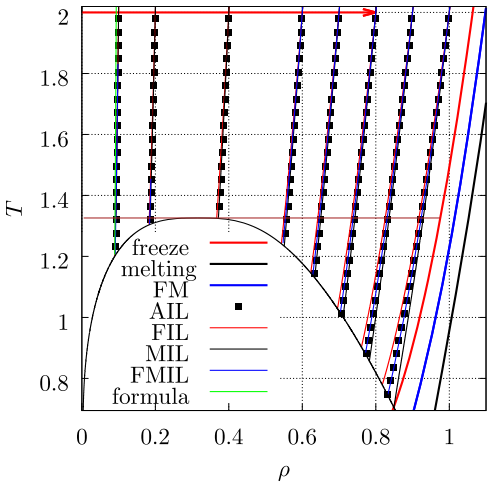

FIG. 2. Four types of predicted configurational adiabat lines according to various prescriptions discussed in the main text. On the right of the figure, the freezing density line is denoted by "freeze," the melting density line is "melting," and the average of these two lines is referred to as "FM." The freezing isomorph line ("FIL") is using the expression in Eq. (1), the melting isomorph line ("MIL") is from Eq. (2), the freezing–melting isomorph line ("FMIL") is also defined in Eq. (2), and the analytic isomorph line ("AIL") is from Eq. (3). Examples of the four lines that pass through the points $\rho_0 = 0.1, 0.2, 0.4, 0.6, 0.7, 0.8, 0.9$, or 1.0 and $T_0 = 2$ are presented. The line "formula" is $\sqrt{2}\rho(\overline{T})$ from the last expression of Eq. (8), where $\rho_0 = 0.1$. The horizontal red line at $T = 2$ and terminating at ρ_0, $T_0 = 0.8, 2.0$ illustrates the isotherm (TIP) stage used in the s_{ex} determination. The horizontal black line marks the boundary between the vapor and liquid state points and the supercritical fluid. The binodal curve is taken from Refs. 31 and 38.

where noting that $\rho = \rho_0$ when $\overline{T} = 1$ and $\rho(\overline{T}) \to \rho_0/\sqrt{2}$ in the zero $\overline{T}$ limit (the analytic solution, not taking account of the binodal metastable region). Therefore, for $T_0 = 2$ and $\rho_0 = 0.1$, $\rho = 0.092$ when $T = 1.2$, and for $\rho_0 = 1$, then $\rho = 0.92$. The magnitude of the temperature shift is smaller for low values of ρ_0 (which makes them appear vertical), even though the ratio ρ/ρ_0 is the same in both cases. This results in the trend that as the density of the isomorph shifts to lower values, the curve appears more vertical in Fig. 2. In fact, for the hard sphere system, all of the isomorph-CA lines *are* vertical, which suggests that in the low density region, the hard sphere system could be considered to be a useful approximation to or reference for the LJ system, apart from inside the LJ binodal (see Ref. 39 for further discussion of this correspondence).

The configurational adiabat which an arbitrary LJ fluid state point, ρ, T, is on (within the AIL approximation) requires the A parameter defined in Eq. (3) for that isomorph to be determined. This involves first calculating the associated reference state point, ρ_0, T_0. From Eq. (3), the starting point is

$$\frac{T}{T_0} = A(\rho_0, T_0)\left(\frac{\rho}{\rho_0}\right)^4 + [1 - A(\rho_0, T_0)]\left(\frac{\rho}{\rho_0}\right)^2. \tag{9}$$

The parameter A can be calculated by solving numerically the expression in Eq. (9) using the predetermined function defined in Eq. (4).

Let T_{ipl4} and ρ_{ipl4} in LJ units be the temperature and density of the AIL in the IPL4 limit. The limiting IPL4 configurational adiabat in the high temperature (density) limit is given by

$$\frac{T}{T_0} \to A(\rho_0, T_0)\left(\frac{\rho}{\rho_0}\right)^4 \equiv \text{const.}, \quad \frac{\rho_{ipl4}^4}{T_{ipl4}} \to \frac{1}{A(\rho_0, T_0)}\frac{\rho_0^4}{T_0} \equiv Y. \tag{10}$$

From Ref. 11, we can propose that the excess entropy along the LJ AIL is constant and equal to its value in the IPL4 limit. The quantity, Y, on the right-hand side of the expression on the last line of Eq. (10) defines which IPL4 configurational adiabat the LJ system at ρ, T tends to in the high temperature limit, within the AIL approximation. Therefore, any analytic formula for s_{ex} along that AIL LJ isomorph must be a unique function of Y. A simplification of Eq. (10) is

$$\frac{\rho_{ipl4}^4}{T_{ipl4}} = \frac{\rho_{ipl4,0}^4}{T_{ipl4,0}}, \tag{11}$$

where $\rho_{ipl4,0} = \rho_0/A^{1/4}$. As $A \geq 1$, the IPL4 isomorph of interest passes through $\rho = \rho_{ipl4,0}$ at $T = T_0 = T_{ipl4}$, which is to the left of ρ_0.

D. Relationship between the AIL, FIL, and MIL procedures

In Fig. 2, the LJ coexisting fluid-phase boundaries given by the essentially exact expressions by Schultz and Kofke are presented.[19,20] There are also approximate expressions for the LJ freezing and melting lines in the literature,[15,23] which take the form $T = A\rho^4 - B\rho^2$. This simple analytic form is only approximate because the freezing and melting lines are already known not to form a single CA, especially for temperatures below about 2.[21,22] Nevertheless, it is of interest to compare the performance of these two formulations for the freezing and melting lines because of the importance of the similar AIL expression for the CA within the fluid phase.

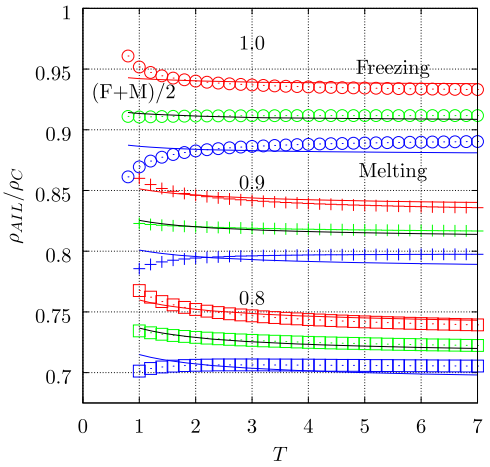

FIG. 3. The ratios ρ_{AIL}/ρ_{fr} ("Freezing"), ρ_{AIL}/ρ_m ("Melting"), and their arithmetic mean ["(F + M)/2"] as a function of temperature are shown. The parameters are $T_0 = 2$ and $\rho_0 = 0.8, 0.9$, and 1.0, which are indicated in the figure. The equation AIL constants are $A = 1.614\,79, 1.546\,41$, and $1.483\,40$, respectively (note B = A-1). The symbols are using the freezing and melting line expressions of Schultz and Kofke,[19,20] and the solid lines are using $T = A\rho^4 - B\rho^2$, where A and B are 2.27 and 0.80 for freezing and 1.76 and 0.69 for melting.[23]

Figure 3 presents the density ratios for the AILs, which pass through $[\rho_0, T_0]$ of [1.0, 2.0], [0.9, 2.0], and [0.8, 2.0], respectively. They all terminate on the liquid side of the vapor–liquid binodal. Note that the melting and freezing lines splay out in opposite directions below a temperature of about 2.0 (see also Fig. 2 in P1). Although there are some differences between the curves derived from the two sources of the freezing and melting lines, which might be expected, their average for the two prescriptions agrees surprisingly well and is relatively flat across the whole temperature range particularly as ρ_0 tends closer to the freezing line. This observation complements and substantiates the conclusions above that an average of the freezing and melting line data mirrors the AIL configurational adiabat line trends quite well.

III. EXCESS ENTROPY DETERMINATION

This section covers the methodology used in this study to determine the excess entropy by molecular dynamics simulation along the AIL, FIL, MIL, and FMIL.

A. Widom's method

The excess entropy per particle, s_{ex}, is defined in terms of u, the excess ("residual") chemical potential, μ_{ex}, or alternatively the excess Helmholtz free energy per particle, a_{ex}, from Ref. 40,

$$\frac{s_{ex}}{k_B} = \beta u - \beta\mu_{ex} + Z - 1 = \beta u - \beta a_{ex}, \tag{12}$$

where $\beta = 1/k_BT$ and the total compressibility factor $Z = P/\rho k_BT$ (P is the pressure and k_B is Boltzmann's constant). Molecular dynamics simulation can be used to compute u and P as ensemble averages, and it therefore remains to determine μ_{ex} or a_{ex} in order to obtain s_{ex}.

Widom's particle insertion method (WM)[41–44] can be used in an NVT MD or Monte Carlo simulation to determine μ_{ex}. Let the interaction energy of a virtual test particle randomly inserted into the N particles in the simulated system be ΔU^+, where both test and host fluid particles interact with the same pair potential. Then,

$$\beta\mu_{ex} = -\ln\langle\exp(-\beta\Delta U^+)\rangle, \tag{13}$$

which together with Eq. (12) can be used to calculate s_{ex}.

As is well-known, the WM is most efficient at fluid densities away from the freezing line, as the probability of inserting a particle becomes less likely with increasing density.

B. Thermodynamic integration

Thermodynamic integration (TI) included in molecular dynamics simulation is another widely used route to obtain free energy and entropy differences [using Eq. (12)], which is computationally efficient for the fluid up to the freezing line. To formulate this method in the most general way, it is convenient to define the quantity $\Pi_{ex} = P_{ex}/\rho^2 = W/\rho$, where W is the virial. Largely following the procedure of van der Hoef in Ref. 45, the starting point of the present treatment is

$$\left(\frac{\partial\beta a_{ex}}{\partial\beta}\right)_\rho = u(\rho,\beta), \left(\frac{\partial a_{ex}}{\partial\rho}\right)_\beta = \Pi_{ex}(\rho,\beta). \tag{14}$$

The value of a_{ex} at any fluid state point ρ,β can be obtained from its value at ρ_0,β_0 using

$$\beta a_{ex}(\rho,\beta) = \beta_0 a_{ex}(\rho_0,\beta_0) + \int_{\beta_0}^{\beta} u(\rho,\beta')d\beta' + \int_{\rho_0}^{\rho} \beta_0\Pi_{ex}(\rho',\beta_0)d\rho', \tag{15}$$

which has separate isochore and isotherm stages. The expression in Eq. (15) can be evaluated numerically by carrying out a series of molecular dynamics simulations for closely spaced values of ρ and β. The combination of isochore ("TIU") and isotherm ("TIP") stages between two arbitrary density and temperature state points, given in Eq. (15), is in this work referred to as the "TIPU" procedure.

From Eq. (15), the desired quantity, $\beta a_{ex}(\rho,\beta)$, can be obtained by integrating along an isotherm from zero density to ρ,[40,46–48]

$$\beta a_{ex}(\rho,\beta) = \int_0^\rho \beta\Pi_{ex}(\rho',\beta)d\rho' = \int_0^\rho \frac{[Z(\rho',\beta)-1]}{\rho'}d\rho', \tag{16}$$

where note that $[Z(\rho',\beta)-1]/\rho' \to b_2$ as $\rho' \to 0$ and b_2 is the second virial coefficient. The $\ln\rho$ term resulting from the integral in the second line of Eq. (16) subtracts off the ideal gas contribution to the Helmholtz free energy.

Both βu and βa_{ex} tend to zero in the $\rho \to 0$ limit for any T. In the high temperature limit, the LJ second virial coefficient converges to that of the IPL4 system, $b_2 = 2^{3/2}\pi\Gamma[3/4]\beta^{1/4}/3$,[12] where $\Gamma[x]$ is the gamma function of x. All the LJ virial coefficients tend to zero in the $\beta \to 0$ limit.

A practical approach that can be used in molecular dynamics simulation to calculate s_{ex} in the liquid region of the phase diagram is to adopt a combination of first (a) the isotherm (TIP) and then the (b) isochore–isotherm (TIPU) route, the latter in simultaneous small steps of density and temperature, as presented in Eqs. (16) and (15), respectively. The TIPU part traces out the isomorph, while the TIP is employed to determine the excess Helmholtz free energy of the reference state point, ρ_0, T_0, from the $\rho \to 0$ limit. The isotherm approach is used at a temperature $T > T_c$ (the critical point temperature) to a density relevant to the liquid region, and then, the isochore–isotherm method is pursued to lower densities, decreasing T (increasing β) into the liquid region using one of the analytic equations put forward in Sec. II. This procedure bypasses the liquid–vapor metastable coexistence region and is illustrated in Fig. 2, which shows the isotherm step at $T = 2$ terminating at $\rho_0 \equiv \rho = 0.8$. The TIPU method is then continued to lower temperature and density until it terminates on the liquid side of the liquid–vapor binodal. The predicted liquid part of the CA is the TIPU part of this path. The extent to which each of these analytic lines satisfies the condition of constant excess entropy was determined from these TI MD simulations.

This combined TIP and TIPU strategy was implemented along the FIL, FMIL, and AIL. The three lines are completely analytic, and they all pass through the same set of ρ_0 and T_0 on the phase diagram, each of which specifies a potential configurational adiabat.

Following the approximations of Zwanzig [Eq. (26) in Ref. 13], it can be shown that both βu and βa_{ex} (and hence s_{ex}) vary as $\sim \rho\beta^{1/4}$ in the $\beta \to 0$ limit. We note also that in the high temperature limit, the one component plasma (OCP) where there are r^{-1} interactions, βu, and inverse power potential systems have been found to have a leading $\beta^{1/4}$ dependence in the $\beta \to 0$ limit.[49–52] Therefore, βu and βa_{ex} tend to zero (i.e., the ideal gas limit) at constant density as $\sim \beta^{1/4}$ in the high temperature limit. Another way of calculating the excess entropy change across an isochore is to fit a set of βu values from MD simulations carried out at a set of temperatures to a low order polynomial in powers of $\beta^{1/4}$, for example,

$$\begin{aligned} \beta u &= A_s\beta^{1/4} + B_s\beta^{1/2} + C_s\beta^{3/4} + D_s\beta, \\ \beta a_{ex} &= \int_0^\beta u(\beta')d\beta' = 4A_s\beta^{1/4} + 2B_s\beta^{1/2} + \frac{4}{3}C_s\beta^{3/4} + D_s\beta, \\ s_{ex}(\beta) &= \beta u - \beta a_{ex} = -3A_s\beta^{1/4} - B_s\beta^{1/2} - \frac{C_s}{3}\beta^{3/4}. \end{aligned} \tag{17}$$

The constants A_s, B_s, C_s, and D_s contain the density dependence and are obtained at each isochore density. Figure 4 shows the values of s_{ex} for four values of ρ_0 at $T_0 = 2$ determined using Eq. (17). For the number of temperatures used in the simulations, the value of s_{ex} from the potential energy fit was found to be sensitive to the temperature range employed but was typically close to the values obtained by the other methods.

These values are statistically indistinguishable from the values obtained by the TIP route, which are also shown in Fig. 4.

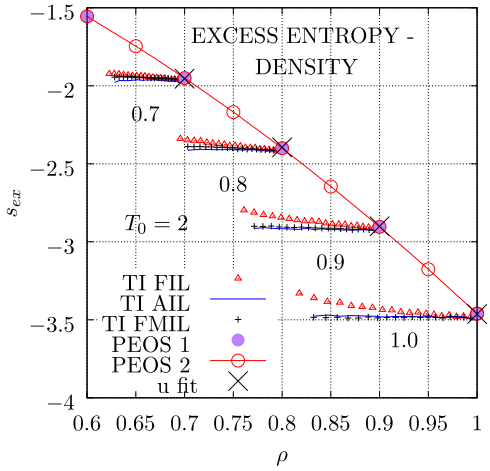

FIG. 4. s_{ex} produced for the three pairs of lines presented in Fig. 2. The various curves pass through the state points $\rho_0 = 0.7, 0.8, 0.9$, and 1.0, and $T_0 = 2$. The curved envelope line in the figure traces out the isotherm part of the simulation sequences, and the roughly horizontal lines are the s_{ex} values for the state points presented in Fig. 2, traced out using the TIPU procedure of Eq. (15), and where $\rho_0 \geq 0.7$. "PEOS 1" and "PEOS 2" are independent implementations of the parameterized equation of the state method.[31] Some data points for the WM ("Widom") are shown. The crosses ("x") labeled "u fit" are from Eq. (17) fitted to the MD simulation potential energy values for temperatures below 80, 16, 16, and 43 at isochore densities 0.7, 0.8, 0.9, and 1.0, respectively. The number of particles in the simulation cell for this and subsequent figures was 500.

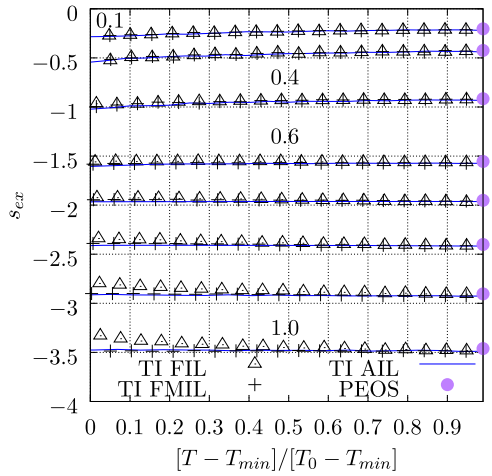

FIG. 5. The s_{ex} values as a function of $[T - T_{min}]/[T_0 - T_{min}]$, where T_{min} is the temperature at which each line intersects the liquid–vapor binodal envelope. The three pairs of line types presented in Fig. 2 are employed with $\rho_0 = 0.1, 0.2, 0.4, 0.6, 0.7, 0.8, 0.9$, and 1.0 from top to bottom. Several values of ρ_0 are shown in the figure, above the associated data in each case. The PEOS[31] predictions along the TIP isotherm part are also shown.

In the past, many of the state points used to test the isomorph scaling have been in the supercritical region, which has tended to obscure any deficiency of FDS for liquid state points. Consequently, the results of simulations presented in this section are in or close to the liquid part of the LJ phase diagram.

Figure 4 compares the s_{ex} values for the three pairs of lines presented in Fig. 2. They start at a density $\rho = \rho_0$ and terminate on the liquid side of the liquid–vapor binodal. The excess entropy values decrease in magnitude as temperature decreases for the FIL case, whereas it is statistically almost constant and the same for the FMIL and AIL. This result indicates that in the liquid part of the phase diagram and the nearby supercritical region, the AIL and FMIL are noticeably closer to being configurational adiabats than those using the freezing density scaling FIL route.

Figure 4 also presents s_{ex} values calculated by Widom's particle insertion method and the PEOS routes. These are along the $T = 2$ isotherm, which forms the envelope of ρ_0 starting state points for the TIPU segments. They are in very good agreement, indicating that the PEOS is sufficiently accurate to explore configurational adiabat and isomorph aspects of the fluid phase diagram within its parameterized temperature and density range.

The format of the s_{ex} data in Fig. 4 is not suitable for revealing the trends exhibited by the FIL, FMIL, and AIL when ρ_0 is less than about the critical point density because they are almost vertical. Figure 5 gives instead the s_{ex} data as a function of $[T - T_{min}]/[T_0 - T_{min}]$, where T_{min} is the temperature where the line intersects the liquid–vapor binodal. This quantity ranges from 0 to 1 as T increases from the binodal temperature to T_0. Figure 5 shows that the FIL s_{ex} for ρ_0 close to the freezing boundary increases slightly as the binodal boundary is approached. The s_{ex} FMIL and AIL are hardly distinguishable within the simulation (standard error) statistics. As the reference density, ρ_0, decreases, the three types of line converge on the scale of Fig. 5. For densities lower than about 0.4, they all show a trend where s_{ex} decreases marginally in magnitude as temperature reduces. It can be concluded that to a good approximation, all the lines in Fig. 5 covering a wide density range are close to being configurational adiabats, as is the case for hard spheres. The similarity between the behavior of hard spheres and the LJ system in the $\rho_0 \to 0$ limit has also been noted recently in Ref. 39.

To summarize this section, it is shown that the AIL formula given in Eq. (3) that employs a *single* value of ρ_0 along the $T_0 = 2$ isotherm specifies the whole of a configurational adiabat line to a good approximation. The AIL $\rho(T)$ curve gives a nearly constant value of s_{ex} along its entire length and performs significantly better in the liquid part of the phase diagram than the FIL formula. The average of the freezing and melting densities at each temperature also gives comparable accuracy to AIL. Both AIL and FMIL give better CA in the liquid part of the phase diagram than freezing density scaling. The three methods are as good as each other for temperatures in excess of about 2 encompassing the gradual transition to the IPL4 limit. The FMIL procedure may be applicable to other model and experimental systems if their freezing and melting lines are known, in contrast to AIL, which in its present form at least, is based on the LJ potential and more generally is not formally dependent on the freezing or melting curves.

C. Analytic formulas from the high temperature AIL limit

It was shown in P2 that in the high temperature limit, the AIL converges to that of the $n = 12$ IPL4 configurational adiabat. The contributions to s_{ex} arising from the repulsive and attractive parts

of the potential scale as $\sim T^{-1/2}$ and cancel each other out in that limit, so s_{ex} is almost constant, as was demonstrated by the MD simulations carried out in P2. As the excess entropy is taken (by definition) to be constant along the AIL, it is only necessary for it to be calculated at one point, which is conveniently chosen to be in the high temperature or "IPL4" limit (if another, lower temperature state point were to be used, another set of A and B parameters would be required, which would unnecessarily complicate the analysis).

The excess entropy of the IPL4 system can be determined using the basic thermodynamic definition given in Eq. (12). The quantity βa_{ex} was obtained by TIP using Eq. (16) and fitted to the analytic formula used by Hansen[12] and Rosenfeld.[1] The excess entropy in units of k_B is

$$-s_{ex,ipl4} = h_1 x + h_2 x^2 + h_3 x^3 - h_{10} x^{10}, \tag{18}$$

where $x = \rho/T^{1/4} \equiv \rho_0/[A(\rho_0, T_0)T_0]^{1/4}$ and h_1, h_2, h_3, and h_{10} are 2.754 91, 1.858 91, 0.753 956, and 0.192 422, respectively. This expression using Hansen's numerical data[12] gives 2.721 75, 1.816 025, 0.874 367, and 0.652 857, respectively, for these constants. A generalization of the Hansen–Rosenfeld formula is

$$s_{ex,ipl4} = \sum_{i=1}^{k} Q_i x^i, \tag{19}$$

where k is the number of terms in the series.

As the IPL4 potential is purely repulsive and reasonably steep, it might be anticipated that an analytic expression for the excess entropy of hard spheres might form the basis for one applicable to the IPL4 system. These MD TI data were also fitted to a generalization of the Carnahan–Starling (CS) formula for the excess entropy of hard spheres,[53] where the two volume fraction coefficients were treated as adjustable parameters,

$$s_{ex,ipl4} = -\frac{a_{ipl}\kappa - b_{ipl}\kappa^2}{(1-\kappa)^2}, \tag{20}$$

where $\kappa = \pi\rho_{ipl4}T_{ipl4}^{-1/4}/6 \equiv \pi\rho_0/6[A(\rho_0, T_0)T_0]^{1/4}$, which follows from Eq. (10). The effective volume fraction, κ, has a temperature dependence, which follows that of an effective hard sphere diameter using Boltzmann's criterion.[54] The constants $a_{ipl} = 5.628\,54$ and $b_{ipl} = 6.161\,85$ were determined by least squares fitting of MD IPL4 ρ data up to the freezing density along the $T = 1$ isotherm.

Equations (18)–(20) reproduce the MD data very well, as may be seen in Fig. 6. Many different functional forms could therefore probably fit the MD data with sufficient accuracy to have practical use because the excess entropy is a relatively weak and monotonically varying function of density. The CS formula given in Eq. (20) is adopted for further use in this work because, although it does not fit the MD data quite as well as the polynomial formulas (see the upper magnified lines in Fig. 6), it has fewer parameters, and as it is adapted from a formula used for hard spheres, it could be claimed to have a more physical basis, which is a great advantage in analytic treatments.

The steps to obtain s_{ex} at an arbitrary LJ fluid state point, ρ, T, are as follows. It is assumed that this state point lies on an AIL isomorph. First, it is necessary to determine the parameter A of this line, using Eqs. (9) and (10). This is achieved numerically by

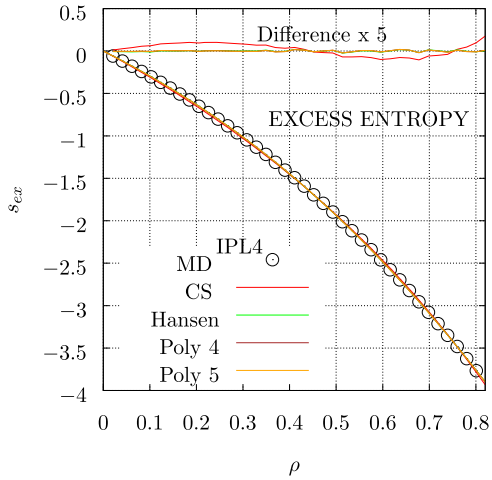

FIG. 6. The excess entropy of the IPL4 system at $T = 1$ obtained by the TIP MD method of Eq. (16) as open circles. The Hansen–Rosenfeld expression of Eq. (18) is "Hansen." The polynomial formula of Eq. (19) for $k = 4$ ("Poly 4") has the parameters $Q_1 \cdots Q_4$, which are −2.785 47, −1.587 85, −1.4613, and 0.570 85, respectively. The $k = 5$ ("Poly 5") case of Eq. (19) is where $Q_1 \cdots Q_5$ are −2.788 85, −1.549 91, −1.598 34, 0.768 826, and −0.099 302 7, respectively. The generalized Carnahan–Starling formula "CS" is the expression in Eq. (20). The lines near the $y = 0$ axis are differences between these analytic fit formulas and the MD values, multiplied by 5.

scanning through the potential ρ_0 range and determining the A parameter for each value of ρ_0 using Eq. (4). The value of A chosen is that which predicts the value of density nearest to ρ at the temperature, T, within a predetermined resolution. The next stage assigns that state point's excess entropy by equating it to that of the limiting IPL4 system, where s_{ex} is given within the AIL approximation by

$$s_{ex,ipl4}\left(\frac{\rho_{ipl4}^4}{T_{ipl4}}\right) = s_{ex,ipl4}\left(\frac{1}{A(\rho_0, T_0)}\frac{\rho_0^4}{T_0}\right) = s_{ex,LJ}(\rho, T). \tag{21}$$

This procedure is illustrated schematically in Fig. 7. Therefore, Eq. (20) gives the excess entropy of any LJ ρ, T fluid state point, within the AIL approximation, once T_0 is defined and the associated ρ_0 and $A(\rho_0, T_0)$ values are determined. The freezing and melting densities of the LJ system at $T = T_0 = 2$ are 1.063 76 and 1.133 05, respectively.[19,20] These are significant values as the AIL reference state points are chosen to be at this temperature.

Figure 8 presents the value of s_{ex} for an evenly distributed selection of LJ fluid state points in the liquid and supercritical fluid regions using the AIL procedure just described, i.e., by identifying which configurational adiabat each LJ point is on and then determining its excess entropy by assigning it to that of the high temperature limiting IPL4 fluid. The state points were those used by Meier to calculate LJ transport coefficients.[55] The densities are plotted normalized by the freezing density at each temperature, $\rho/\rho_{fr}(T)$. Figure 8 shows that the AIL procedure for calculating $s_{ex}(\rho, T)$ for this dataset obeys well the expression in Eq. (20), which can therefore be considered to be a generally accurate representation of the

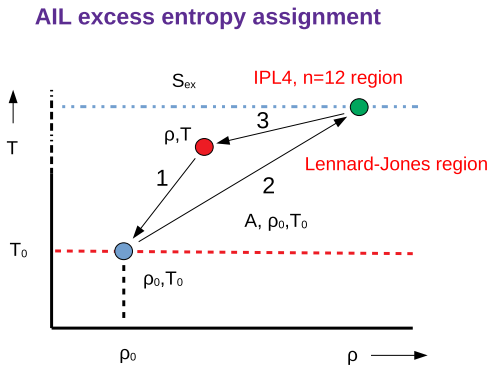

FIG. 7. Schematic diagram illustrating the three stages path on the ρ, T plane used to assign a value of s_{ex} to a point in the ρ, T plane via the AIL procedure. The first stage ("1" in the figure) is to assign a value of ρ_0 and $A(\rho_0, T_0)$ on the $T = T_0$ isotherm. The second stage ("2") is to assign the value of s_{ex} of that AIL by equating it to that of the IPL4 or $T \to \infty$ LJ AIL limit. Within this approximation, the state point ρ, T also has the same value of the excess entropy, as indicated by the assignment labeled "3" on the figure. The three filled circle symbols are on the same configurational adiabat.

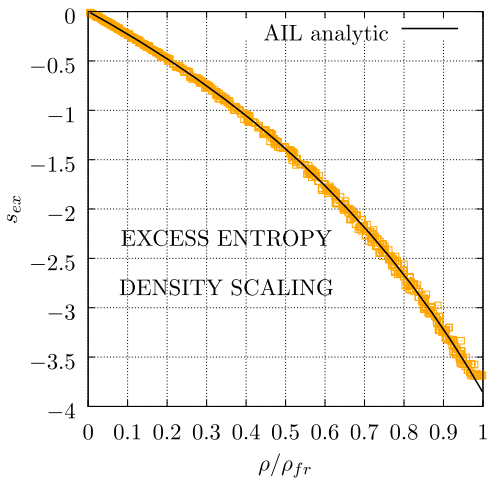

FIG. 8. The dependence of s_{ex} on ρ/ρ_{fr} using the Meier ρ, T data points, which are distributed in the liquid and supercritical regions.[55] The s_{ex} values are obtained using Eqs. (9), (10), and (21). The continuous black line is Eq. (20) taking $T_0 = 2$.

excess entropy over the fluid phase. Figure 8 also shows that for the LJ fluid, the excess entropy and ρ/ρ_{fr} are strongly correlated, as was also shown in Ref. 17.

IV. ISODYNES

It is shown in Figs. 4 and 5 that the AIL and FMIL formulas give essentially perfect configurational adiabats in the liquid region, but FIL does not. It is of interest to compare the transport coefficients along these lines. It might be expected that, for example, the shear viscosity, η_s, in MU should be constant along the AIL and FMIL but not those using the FIL prescription.

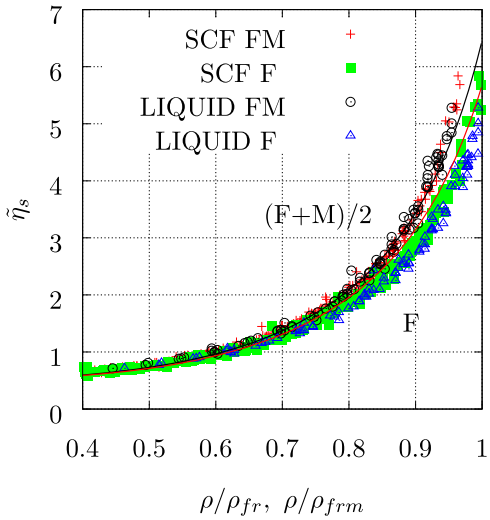

FIG. 9. Comparison of the scaling of the shear viscosity above ("SCF") and below ("LIQUID") the critical temperature. Freezing ("F") and freezing–melting ["(F + M)/2"] density scaling datasets are presented, where $\rho_{frm} = (\rho_{fr} + \rho_m)/2$. The solid lines are $\tilde{\eta}_{s,ip}(\rho)$ from Eq. (23). The black line is with the (F + M)/2 scaling, and the red line is density normalized using the F scaling. The MD shear viscosity data were taken from various sources.[56–60]

Figure 9 presents the reduced shear viscosity in MU, $\tilde{\eta}_s = \eta_s \rho^{-2/3} T^{-1/2}$, against the scaled density, using the freezing density (FIL) and the arithmetic mean of the freezing and melting (FMIL) normalization of the density. The datasets taken from the literature are separated into two parts, one for state points in the liquid region (i.e., below the T_c) and those in the supercritical fluid part. Figure 9 shows that $\tilde{\eta}_s$ are statistically the same above and below the critical temperature using FMIL, but they are systematically lower in the liquid region when FIL scaling is used, especially close to freezing. This indicates that the FIL reduced density scaling leads to different $\tilde{\eta}_s$ curves above and below the critical temperature.

A more systematic investigation of these differences was made here by carrying out equilibrium MD simulations of the shear viscosity, η_s, self-diffusion coefficient, D, and thermal conductivity, λ, along the AIL, FMIL, and FIL for $T < 2$ with the state points employed in Figs. 4 and 5 for some of the values of ρ_0.

Figure 10 shows the MU-scaled transport coefficients, $\tilde{\eta}_s$, $\tilde{D} = D\rho^{1/3} T^{-1/2}$, and thermal conductivity, $\tilde{\lambda} = \lambda \rho^{-2/3} T^{-1/2}$, against the temperature measure of the state point used in Fig. 5. The reference state point $\rho_0 = 1.0$ and $T_0 = 2.0$ are not far from the freezing line. The data shown are the average of the Einstein–Kubo–Helfand[61,62] and Green–Kubo[3] values. The data in Fig. 10 are the block averages of five independent simulations each of 2×10^6 time steps, with $N = 1000$.

Figure 10 reveals that the AIL and FMIL transport coefficients are in very good agreement and constant in MU reduced units along this part of the isomorph. In contrast for FIL, the diffusion coefficient increases and the shear viscosity decreases as the temperature decreases toward the liquid–vapor binodal curve. This is as might be expected as the density of the system decreases to a greater extent

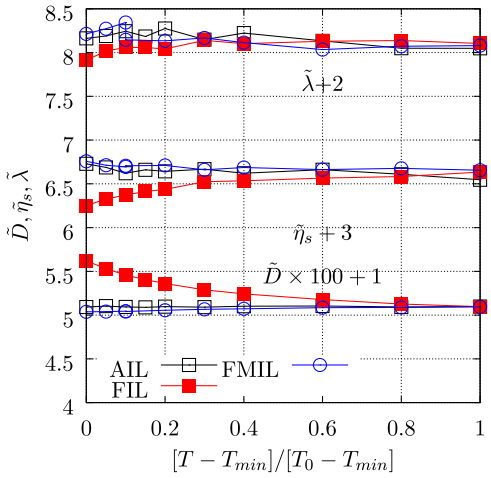

FIG. 10. The $\tilde{D}$, $\tilde{\eta}_s$, and $\tilde{\lambda}$ values as a function of $[T - T_{\min}]/[T_0 - T_{\min}]$ are plotted, where $T_{\min}$ is the temperature where each line intersects with the liquid–vapor binodal curve. The three pairs of lines presented in Fig. 2 using $\rho_0 = 1.0$ are presented. Every symbol is the average of five MD simulations each of 2×10^6 time steps using $N = 1000$.

than along the AIL and FMIL, which are statistically indistinguishable in that respect. The thermal conductivity trends in Fig. 10 also show a more constant MU-reduced value along the AIL and FMIL, although the differences from the FIL scaled data are not so pronounced as for the other two transport coefficients. It has already been noted that the thermal conductivity is mainly determined by the density [see, for example, Fig. 13(a) in Ref. 3] and to a greater extent than for η_s and D. This relative insensitivity to local structure (which might be caused by temperature changes) is also consistent with the fact that Enskog's theory for hard sphere fluids applies remarkably well for the λ of crystalline solids.[63]

Therefore, there is a strong correlation between lines of constant excess entropy and lines of constant transport coefficient when cast in MU reduced units, which supports the conclusion that, to a good approximation, isodynes are also lines of constant excess entropy. This holds for the simple LJ model system, but is not valid for more complex molecular systems with thermally accessible internal degrees of freedom.[9]

A. Prediction of LJ η_s and D from IPL4

First, consider the issue of units. If $\rho_{ipl} = (N/V)\sigma_{ipl}^3$ and $\rho_{LJ} = (N/V)\sigma^3$, the relationship between quantities in IPL and LJ units is for the number density, $\rho \equiv \rho_{LJ} = \rho_{ipl}/\sqrt{2}$, for time, $t_{LJ} = t_{ipl}/2^{1/6}$, for the shear viscosity, $\eta_{s,LJ} = \eta_{s,ipl}/2^{1/3}$, for the self-diffusion coefficient, $D_{LJ} = 2^{1/6} D_{ipl}$, and for the thermal conductivity, $\lambda_{LJ} = \lambda_{ipl}/2^{1/3}$. These differences are a consequence of factor 4 in front of ε in the definition of the LJ potential.

It is of interest to investigate to what extent the transport coefficients of a wide range of equilibrium LJ fluid state points in the liquid and supercritical regions obtained by MD can be predicted from those of the IPL4 system.

The assumption is that along a LJ configurational adiabat for the transport coefficient, X, the value of $\tilde{X}$ is a constant, which is, therefore, also equal to that of the IPL4 system to which the LJ system tends to at high temperature. Section III C describes the procedure for identifying the IPL4 limit for any LJ state point ρ, T. Then, for the shear viscosity in LJ units,

$$\begin{aligned}\eta_s(\rho,T) &= \tilde{\eta}_s \rho^{2/3} T^{1/2} \\ &\simeq \tilde{\eta}_{s,ipl4} \rho^{2/3} T^{1/2} \\ &= \tilde{\eta}_{s,ipl4} \rho_0^{2/3} T^{1/2} \left(\frac{(A-1) + \sqrt{(1-A)^2 + 4AT/T_0}}{2A} \right)^{1/3},\end{aligned} \tag{22}$$

where $\tilde{\eta}_{s,ipl4}$ [from Eq. (21)] is a function of ρ_0 and T_0 and is, therefore, a function of the AIL parameter A, ρ, and T. Equation (7) has been used to remove ρ in the second line to give the expression on lines 3 and 4 of the above equation. The shear viscosity in LJ MU at the IPL4 state point, (ρ_{ipl4}, T_{ipl4}), is $\tilde{\eta}_{s,ipl4}$, and as $T_0 = 2$ is used throughout this work, the A fit parameters given below Eq. (4) can be used. A similar formula was applied in Ref. 23 to the shear viscosity along the LJ freezing line, where $\tilde{\eta}_{s,ipl4}$ in the last line of Eq. (22) was replaced by a constant value of $\tilde{\eta}_s$ and the freezing line was represented by the formula $T = A\rho^4 - B\rho^2$.

Figure 11 shows the density dependence of the IPL4 fluid system shear viscosity when $T = 1$. The shear viscosity was obtained in MD simulation using the Green–Kubo method. These data apply to arbitrary IPL4 state points by replacing ρ_{ipl4} on the abscissa of Fig. 11 by $x \equiv \rho_{ipl4}/T_{ipl4}^{1/4}$. Figure 11 also shows a least squares fit to these data using the functional forms

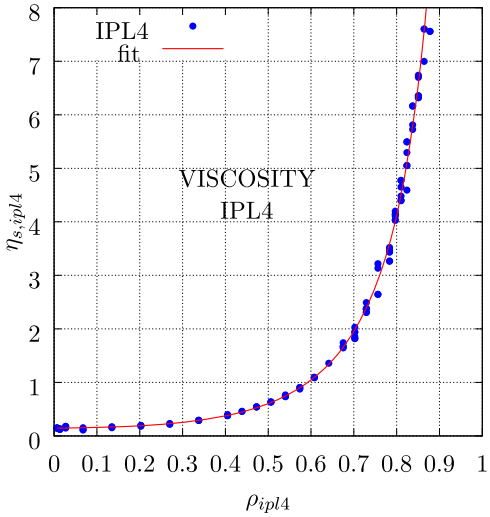

FIG. 11. The density dependence of the IPL4 $n = 12$ fluid system shear viscosity, $\eta_{s,ipl4}$, in LJ units, when $T_{ipl4} = 1$. The shear viscosity was obtained in MD simulation using the Green–Kubo method. A least squares fit to these data using Eq. (23) is also shown, where $a_{v,0} \cdots a_{v,5}$ are −0.385 945, −0.732 810, −0.582 181, 0.531 448, 0.964 694, and 1.578 649. The MD simulations on $N = 2048$ particles were typically for 2800 LJ time units.

$$\eta_{s,ipl4}(x) = a_{v,0} + a_{v,1}x + a_{v,2}x^2 + a_{v,3}[1 - a_{v,4}x]^{-a_{v,5}},$$
$$\tilde{\eta}_{s,ipl4} = \eta_{s,ipl4}(\rho_{ipl4}, T_{ipl4})/\rho_{ipl4}^{2/3} T_{ipl4}^{1/2}, \quad (23)$$

where all quantities are in LJ units. The quantity $\tilde{\eta}_{s,ipl4}$ defined in Eq. (23) is a constant for a given AIL and is used in Eq. (22). The ρ_{ipl4} density is a function of T_{ipl4}, ρ_0, and T_0. The fit function in Eq. (23) [which is inspired by Eq. (19) in Ref. 66] is only meant to represent the MD simulation data for $x > 0$. The values of the constants (given in the caption of Fig. 11) have no intended physical significance.

Therefore, the procedure for assigning a predicted value for the shear viscosity at an arbitrary LJ fluid state point (ρ, T) is first to determine the parameter A and hence the high temperature limiting IPL4 state. Then, the viscosity $\eta_{s,ipl4}$ of the IPL4 system in LJ units is determined using Eq. (23) and finally $\eta_s(\rho, T)$ for the LJ system using the approximation given in the second line of Eq. (22).

Figure 12 presents a correlation plot of the values of $\eta_s(\rho, T)$ for the LJ system using Eq. (22) on the ordinate axis and the values determined directly from MD with the Green–Kubo method. Figure 12 shows that there is a reasonably good one-to-one correlation between the two viscosities, which indicates that the MD LJ shear viscosity values at any part of the fluid phase diagram can be determined to within several percent by this analytic procedure without recourse to MD simulation. This applies to both supercritical fluids and the liquid state points.

Figure 12 also shows an application of the same procedure based on the IPL4 viscosity to predict experimental data for fluid argon using the fit to literature experimental viscosities by Younglove and Hanley (YH).[64] The LJ state points were mapped onto equivalent ones for experimental argon in real units. This was conducted using the respective critical point parameters in their own units $\rho_{\mathrm{Ar}} = \rho_{LJ}\rho_{\mathrm{Ar},c}/\rho_{LJ,c}$ and $T_{\mathrm{Ar}} = T_{LJ}T_{\mathrm{Ar},c}/T_{LJ,c}$. Then, the argon experimental viscosities from the YH fit formula at these "experimental" state points were converted back to LJ units using LJ parameters (see the caption of Fig. 12) for liquid argon employed in simulations. The agreement between the two sets of viscosity data, one based on simulation and the other based on the experiment, is very good from low near gas-like densities to liquid density states (from left to right in Fig. 12). There are a few outlier points, which are systematically low, which may be due to deficiencies in the state point mapping procedure as the LJ and argon phase diagrams will not be exactly superimposable. The LJ parameters are for an effective potential, and also, there may have been regions of the phase diagram where the experimental viscosity data were more limited, which would have adversely affected the quality of the fit in those regions. It might also be related to the fact that LJ is pairwise, while for real argon, higher-order terms in the interactions could be relevant.

There are departures from the linear correspondence between predicted and MD viscosity at low densities, as may be seen in Fig. 13, which shows the same LJ data on a log–log scale. The IPL4 data deviate from the straight line and tend to a limiting value given by kinetic theory for a dilute IPL4 gas with $n = 12$. This deviation from the linear relationship between the viscosities of the IPL4 and LJ systems at low densities is a consequence of the different limiting dilute gas viscosities for the IPL4 and LJ systems as they have a different temperature dependence. The experimental argon viscosity data in Fig. 13 are hardly distinguishable from those of the model LJ particles and notably follow the leveling off of the values in the zero density limit where classical kinetic theory dominates.

The formulas in Eq. (23) used in conjunction with the freezing and melting line densities are the continuous lines in Fig. (9). The prediction is reasonably good although not as good as might

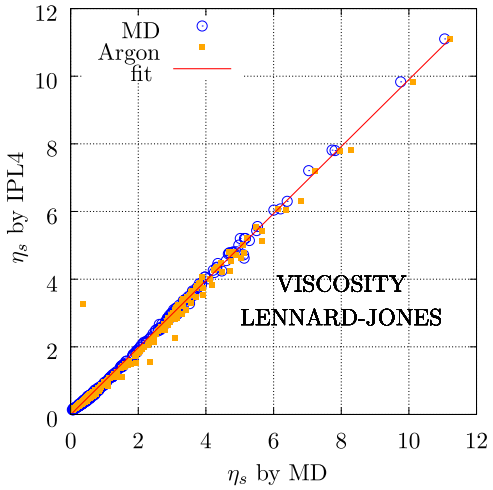

FIG. 12. The predicted $\eta_s(\rho, T)$ for the LJ system using Eq. (22) on the ordinate axis compared to the MD values on the abscissa, which are those taken from the MD simulations in Ref. 55 and the simulation data points used to produce Fig. 10. Data for argon from the parameterized fit to experimental viscosity values in Ref. 64 are shown as orange symbols ("Argon"). The LJ state points are converted to equivalent real unit values for experimental argon, as explained in the main text. The experimental viscosity is then converted to LJ units using $\varepsilon/k_B = 120$ K and $\sigma = 0.3405$ nm,[65] which are the constants used in MD simulations, and these predicted argon viscosity values are presented in the figure. The linear regression fit to the LJ data (blue symbols) has an intercept and slopes of −0.007(9) and 0.991(2).

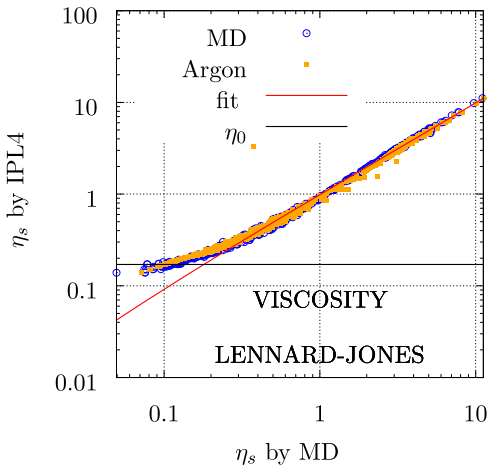

FIG. 13. The same as Fig. 12, except that the data are given on a log–log scale. The black horizontal line is the predicted kinetic theory IPL4 viscosity in the zero density limit, η_0.[67]

have been expected from AIL MD correlation shown in Fig. 12. The freezing–melting ["(F + M)/2"] density scaled datasets from MD are higher than the predictions of Eq. (23) at the highest densities. This discrepancy is presumable because there is an additional approximation required in treating the MD data in Fig. (9) compared with the analysis of Fig. 12, i.e., that the LJ MD state point densities are normalized by the freezing or mean freezing–melting densities. The advantage of using the AIL-based viscosity predictive method of Fig. 12 is that it is not reliant on fluid–solid coexistence density scaling.

The corresponding procedure for the LJ self-diffusion coefficient, D, is

$$D(\rho,T) = \tilde{D}\rho^{-1/3}T^{1/2} \simeq \tilde{D}_{ipl4}\rho^{-1/3}T^{1/2},$$
$$D(\rho,T) \simeq \tilde{D}_{ipl4}\rho_0^{-1/3}T^{1/2}\left(\frac{(A-1)+\sqrt{(1-A)^2+4AT/T_0}}{2A}\right)^{-1/6}, \quad (24)$$

where $\tilde{D}_{ipl4}$ is the self-diffusion coefficient of the limiting IPL4 system in MU. Figure 14 shows the IPL4 D^{-1}_{ipl4} obtained by $T_{ipl4} = 1$ ($i.e., \rho_{ipl4}/T^{1/4}_{ipl4} \equiv \rho_{ipl4}$) Green–Kubo MD and a least squares fit of the analytic form

$$D^{-1}_{ipl4} = a_{d,0} + a_{d,1}x + a_{d,2}x^2 + a_{d,3}[1 - a_{d,4}x]^{-a_{d,5}},$$
$$\tilde{D}_{ipl4} = D_{ipl4}(\rho_{ip})\rho_{ip}^{1/3}/T^{1/2}_{ipl4}, \quad (25)$$

where $\eta_{s,ipl4}$ in Eq. (23) is replaced by $1/D_{ipl4}$. In Fig. 14, $1/D_{ipl4}$ is plotted as a function of ρ_{ipl4} for the temperature $T_{ipl4} = 1.0$. The substitution of the shear viscosity by the inverse self-diffusion coefficient has often been made in the literature, and it is also qualitatively consistent with the Stokes–Einstein relationship at constant temperature.

The D values were not corrected for system size dependence.[63] Very large systems are required to ensure a reliable extrapolation to the limit of an infinite number of particles, N, in the simulation cell.[63] Yeh and Hummer derived an expression based on hydrodynamic arguments for the system size dependence of the self-diffusion coefficient of molecular liquids, which they tested for model water and LJ fluids[68] and which was also used in a recent work on $D(N)$ of model water by Khrapak.[69] In the present context, the diffusion coefficient for LJ systems is predicted from an "equivalent" IPL4 system both using $N \simeq 2000$ in the MD simulations. It is reasonable to assume that the N-correction factor should be similar in the two cases.

The values of the constant formulas in Eqs. (23) (viscosity) and (25) (inverse self-diffusion coefficient) are given in the captions of Figs. 11 and 14, respectively. The last term in each expression is the dominant one as it captures the rapid increase in η_s and $1/D$ (respectively) close to the freezing density. One may consider the effect of the negative constant terms in these formulas to compensate for the effects of the dominant term at low densities. These formulas were developed to represent the IPL simulation data by an analytic expression to be used in the IPL4 to LJ mapping procedure.

Figure 15 shows that correlation between the IPL4 predicted and actual MD derived (inverse) self-diffusion coefficient is very good. This form of presentation is also a useful way of isolating outlier MD points (e.g., the two high density points at the top right-hand corner of Fig. 15), which might be difficult to discern in other ways of presenting such data.

Some of the MD transport coefficient data evaluated for this work and used in Figs. 10–15 are given in the supplementary material.

It was shown by Costigliola *et al.* in Ref. 70 that for a LJ fluid system in the vicinity of the freezing line, the product $\tilde{D}\tilde{\eta}_s$, which is the Stokes–Einstein relation not based on a hydrodynamic diameter,

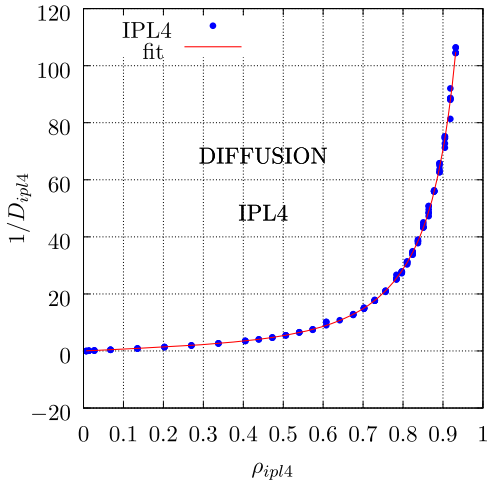

FIG. 14. The density dependence of the IPL4 $n = 12$ fluid system inverse self-diffusion coefficient, D^{-1}_{ipl4}, when $T_{ipl4} = 1$ and where $\rho \equiv \rho_{ipl4}$. D_{ipl4} was obtained in MD simulation using the Green–Kubo method. A least squares fit to these data using Eq. (25) is also shown, where $a_{d,0} \cdots a_{d,5}$ are −5.608 19, −0.587 79, −9.488 86, 5.608 19, 0.959 87, and 1.359 55, respectively.

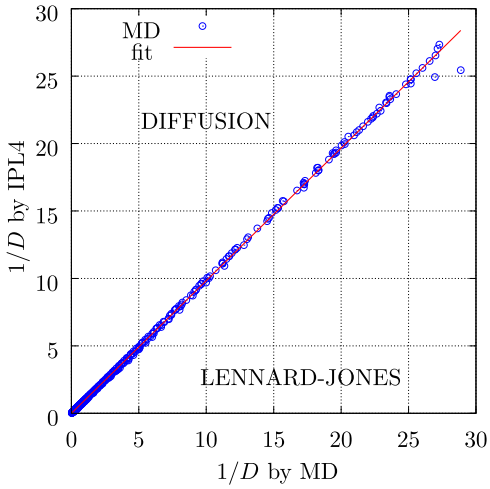

FIG. 15. The same as Fig. 12, except that the inverse diffusion coefficient is considered.

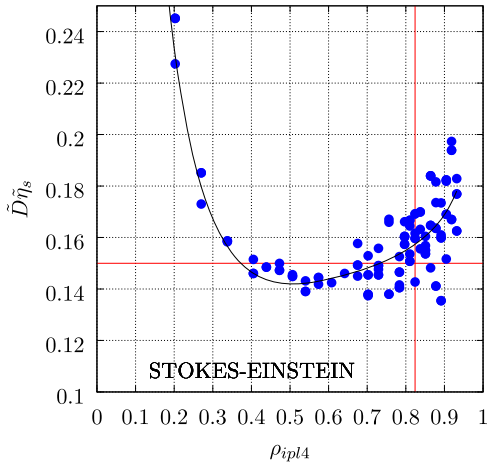

FIG. 16. Test of the Stokes–Einstein relation not based on a hydrodynamic diameter for the IPL4 data given in Figs. 11 and 14 for self-diffusion and shear viscosity, respectively. The quantities expressed in MU, $\tilde{D}\tilde{\eta}_s = D\eta_s/\rho^{1/3}T$, are plotted (blue symbols). The continuous black curve is the same quantity derived from the least squares fits to the MD data specified in Eqs. (23) and (25). The horizontal red line denotes a typical literature value for this quantity near freezing. The vertical red line denotes the freezing density boundary.

converges to a value ~0.15 [see Figs. 2(c) and 2(d) in that publication]. This was shown by others in subsequent publications to be obeyed for a diverse range of model fluids.[9,71] Figure 16 presents the dependence of this quantity as a function of density for the IPL4 fluid system. The self-diffusion and shear viscosity values shown are those taken from Figs. 11 and 14, respectively. Figure 16 confirms that the IPL4 D and η_s MD data of this work are consistent with the Stokes–Einstein relation expressed in MU.

Figure 16 demonstrates that the quantity $\tilde{D}\tilde{\eta}_s$ is in the range 0.15 ± 0.1 in the medium to high density range, which agrees with the previous publication conclusions. There is some scatter in individual data points, which comes mainly from the viscosity values, as the statistics are better for the self-diffusion coefficient. There is evidence that for this model system, the product gradually increases as the system passes through the freezing transition into the metastable fluid region.

B. Origins of the configurational adiabat η_s and D scaling

It is shown here that the AIL LJ lines are to a good approximation also lines of constant excess entropy and isodynes (i.e., constant η_s and D in MU). In addition, the properties of the high temperature (density) IPL4 system give the s_{ex}, $\tilde{\eta}_s$, and $\tilde{D}$ values along the AIL (e.g., see Fig. 15). This indicates that the limiting (purely repulsive) part of the LJ potential and its properties are sufficient to predict s_{ex}, $\tilde{\eta}_s$, and $\tilde{D}$ in the supercritical LJ fluid and liquid state regions to a good approximation, except if the density is essentially in the gas-like regime where systematic deviations are seen (see Fig. 13). The FMIL formulas also serve the same function, as the freezing and melting densities tend to those of the same IPL4 system at high temperature.

This behavior applies even at quite low densities (but not too low), much less than the critical point density, where the system is not strongly correlated (i.e., where the virial-potential energy correlation coefficient is much less than 1[2]) and a harmonic cell model approximation might not be expected to apply well either.

At low densities, in addition to the particle diameter, another length scale (the mean distance between collisions) enters the description. The statistical thermodynamics and transport behavior in this density region become more determined by the repulsive part of the potential, while the contribution from the attractive part of the potential could be approximated by a uniform background, which does not affect the dynamics of the particles significantly. This trend was also noted in Ref. 39 in which the isodyne behavior of hard spheres and the Lennard-Jones fluids was compared. The transport coefficients of IPL fluids at low density can be represented well using Enskog theory expressed in terms of a temperature dependent effective hard sphere diameter, which is weakly dependent on the IPL exponent, n.[67] Note that for the hard sphere system, configurational adiabats are isochores.

At high densities, the particles are closely packed together and perturbation theories (PTs) of the liquid state may explain why s_{ex}, $\tilde{\eta}_s$, and $\tilde{D}$ are constant along the AIL and FMIL in that part of the fluid phase diagram. A perturbation theory of the liquid state assumes that the structure of the liquid is determined by the repulsive part of the pair potential, and the contribution from any attractive part can be added on in an approximate way by calculating its contribution from the liquid structure (e.g., via the radial distribution function) generated solely by the repulsive part of the potential.[72] From Eq. (12), we have $s_{ex}/k_B = \beta u - \beta a_{ex}$, and therefore, within the PT framework, $\beta a_{ex} = \beta a_{r,ex} + \beta u_{a,r}$, where $u_{a,r}$ is the attractive ("a") part of the potential from a system generated from the repulsive ("r") part. The repulsive part of the LJ potential is used as the reference system. Bearing in mind these are approximations, for the LJ system,

$$\begin{aligned} s_{ex}/k_B &= \beta u - \beta a_{ex} \\ &= \beta u_r + \beta u_{a,r} - [\beta a_{r,ex} + \beta u_{a,r}] \\ &= \beta u_r - \beta a_{r,ex}, \end{aligned} \tag{26}$$

which shows that within the PT approximation, the excess entropy of the LJ system only depends on the properties of the purely repulsive reference state [i.e., here that of the high temperature (density) limiting IPL4 fluid]. This approximation, as discovered, is quite well obeyed along the FMIL and AIL, in the liquid part of the phase diagram. In contrast, other PT defined quantities such as u and a_{ex} have a contribution from the attractive part of the potential, making s_{ex} unique in this respect.

C. Rosenfeld excess entropy scaling theory

This strong correlation between transport coefficients and excess entropy is already well-known in another context, as is demonstrated in the Rosenfeld plots given in Fig. 17 using the MD data of Meier.[55] The reduced transport coefficients $\tilde{X} \equiv \tilde{D}^{-1}$, $\tilde{\eta}_s$, and $\tilde{\lambda}$ are presented, which show a transition from gas- to liquid-like behavior from left to right on either side of the minimum.[10] The data in the high density regime limit comply well with the relationship $\tilde{X} = A \exp(-bs_{ex})$ with constants for each transport coefficient given in the caption of Fig. 17. The literature b values of −0.8 (for $\tilde{D}$), 0.8, and 0.5, respectively,[67,73] are statistically close to those given in the caption of Fig. 17. Figure 17 highlights the similarity in the excess

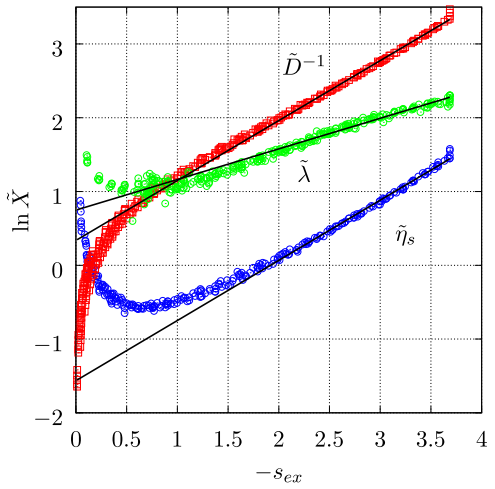

FIG. 17. The dependence of the three transport coefficients in MU units, $\tilde{X} \equiv \tilde{D}, \tilde{\eta}_s$ and $\tilde{\lambda}$, obtained by MD,[55] on excess entropy for the LJ system. The quantity $\tilde{D}^{-1}$ is plotted instead of $\tilde{D}$. These data were fitted to the data for $-s_{ex} \geq 2$ using Rosenfeld's analytic form given in the main text. The constants for A and b are 0.714 and −0.812(4) for $\tilde{D}$, 0.209 and 0.815(6) for $\tilde{\eta}_s$, and 2.111 and 0.415(6) for $\tilde{\lambda}$.

entropy dependence of $\tilde{D}^{-1}$ and $\tilde{\eta}_s$. The viscosity and thermal conductivity coefficients at $s_{ex} \simeq -0.7$ correspond to a crossover between gas-like and liquid-like regions on the phase diagram, which has been discussed previously in the literature.[16,74]

Bell *et al.* carried out a comprehensive investigation of the dependence of the LJ transport coefficients on the excess entropy.[75] Simulation data for the transport coefficients were plotted as a function of s_{ex} derived from a parameterized LJ equation of state. Correlations typical of the Rosenfeld form were found to agree in certain regions of the fluid phase diagram. We consider that the AIL method is particularly accurate in this general field and has the advantage that it bypasses the need to compute the excess entropy, which is generally a time consuming activity (the Lennard-Jones system is particularly fortunate in this respect as there are many accurate analytic equations of state for the fluid phase). The present AIL method extracts the LJ transport coefficient from an already determined IPL value using a formal mapping procedure. The transport coefficients of one model system are mapped onto those of another without explicitly employing the excess entropy (although it is implicitly involved in the underpinning theoretical formulation).

V. CONCLUSIONS

It is shown in this study that the harmonic model line (AIL) on the fluid phase diagram of the Lennard-Jones fluid, proposed in P2, and a variant of freezing density scaling, where the average of the freezing and melting densities (FMIL) is taken instead, give essentially the same constant value for the excess entropy s_{ex} even down to the liquid–vapor binodal. The AIL method has the advantage that the excess entropy of the LJ system is essentially analytic when the excess entropy of the high temperature (density) limiting inverse power value is incorporated in the treatment. The freezing density scaling (FIL) lines do not exhibit constant excess entropy to the same extent in the liquid region, particularly when close to the freezing line and the liquid binodal boundary. The three lines at all densities converge to essentially the same line for temperatures much in excess of the critical temperature.

The self-diffusion coefficient, shear viscosity, and thermal conductivity of the Lennard-Jones fluid in the liquid and supercritical regions when expressed in macroscopic units are constant to a good approximation along each configurational adiabat. This observation is consistent with the classical perturbation theory of liquids, at least at high density.[76]

A practical outcome of this work is that it has been shown that the self-diffusion coefficient and shear viscosity of the Lennard-Jones fluid at essentially any state point (apart from at extremely low densities where the system is described well by kinetic theory) can be predicted quite well from their high temperature (density) configurational adiabat limits, which can be represented well by those of the associated inverse power potential system. Owing to the system parameterization formulations generated in this work, this assignment is now largely an analytic exercise, without requiring any further simulations. Figure 12 demonstrates that the same correlation exists between the IPL viscosity and experimental argon viscosity data, which suggests that the IPL prediction scheme could be reasonably accurate for other small molecule fluids, which can be represented quite well by the Lennard-Jones potential.

Another potentially useful practical feature of this work is the formula for the excess entropy along a LJ configurational adiabat, which is taken to be that of the high temperature limiting IPL s_{ex} system. This is stated in Eq. (21). The IPL s_{ex} can be parameterized independently by simulations along one of its isotherms, for example.

The advantage of the isomorph–isodyne description of liquids is that its coarse-grained or "top down" quasi-thermodynamic basis means that, in principle, it could be applied to a wide range of fluids without requiring any specific molecular level detail for each chemical system. It is generic in that respect. There may be applications of the treatments in this work in the fields of geology, rheology, and tribology, for example, particularly where high temperatures and pressures are involved (when the system is closer to the inverse power configurational adiabat limit). The analysis and theoretical description of the observed phenomena could then possibly be simplified, for example, the analytic description might be reduced in dimensionality.

SUPPLEMENTARY MATERIAL

The supplementary material contains the molecular dynamics simulation thermodynamic and transport coefficient data used to generate some of the figures in this work.

ACKNOWLEDGMENTS

D.D. acknowledges a Shell/RAEng Research Chair in Complex Engineering Interfaces and the EPSRC Prosperity Partnership inFUSE EP/V038044/1. D.D. and D.M.H. acknowledge the support received from the EPSRC under the Established Career Fellowship, Grant No. EP/N025954/1. L.C. carried out this work while an academic visitor at Imperial College London and acknowledges the support from the VILLUM Foundation's Matter, Grant No. (VIL16515).

AUTHOR DECLARATIONS

Conflict of Interest

The authors have no conflicts to disclose.

Author Contributions

D. M. Heyes: Conceptualization (equal); Data curation (equal); Formal analysis (equal); Investigation (equal); Methodology (equal); Resources (equal); Software (equal); Validation (equal); Visualization (equal); Writing – original draft (equal). **D. Dini**: Conceptualization (equal); Funding acquisition (equal); Investigation (equal); Methodology (equal); Project administration (equal); Resources (equal); Supervision (equal); Writing – original draft (equal). **S. Pieprzyk**: Conceptualization (equal); Data curation (equal); Formal analysis (equal); Investigation (equal); Methodology (equal); Validation (equal); Writing – original draft (equal). **A. C. Brańka**: Conceptualization (equal); Formal analysis (equal); Investigation (equal); Methodology (equal); Validation (equal); Writing – original draft (equal). **L. Costigliola**: Conceptualization (equal); Formal analysis (equal); Investigation (equal); Methodology (equal); Writing – original draft (equal).

DATA AVAILABILITY

The data that support the findings of this study can be obtained from the corresponding author upon reasonable request.

APPENDIX: SUMMARY OF ACRONYMS USED IN THIS WORK

Table I gives a list of the acronyms used in the text and what they stand for.

TABLE I. A list of the acronyms and their definitions used in this work.

Acronym	Definition
CA	Configurational adiabat
MD	Molecular dynamics
MU	Macroscopic reduced units
IPL	Inverse power potential
IPL4	IPL with 4 prefactor and $n = 12$
WM	Widom's method
LJ	Lennard-Jones
PT	Perturbation theory
TI	Thermodynamic integration
TIP	TI pressure isotherm route
TIU	TI potential energy isochore route
TIPU	TI pressure isochore–isotherm route
FDS	Freezing density scaling
FIL	Freezing CA line
MIL	Melting CA line
FMIL	Freezing–melting CA line
AIL	Analytic isomorph line
PEOS	Parameterized equation of state
MBWR	Modified Benedict–Webb–Rubin PEOS
YH	Younglove and Hanley

REFERENCES

[1] Y. Rosenfeld, Phys. Rev. A **15**, 2545 (1977).
[2] N. Gnan, T. B. Schrøder, U. R. Pedersen, N. P. Bailey, and J. C. Dyre, J. Chem. Phys. **131**, 234504 (2009).
[3] D. M. Heyes, D. Dini, L. Costigliola, and J. C. Dyre, J. Chem. Phys. **151**, 204502 (2019).
[4] T. S. Ingebrigtsen, T. B. Schrøder, and J. C. Dyre, Phys. Rev. X **2**, 011011 (2012).
[5] T. S. Ingebrigtsen, L. Bøhling, T. B. Schrøder, and J. C. Dyre, J. Chem. Phys. **136**, 061102 (2012).
[6] J. C. Dyre, J. Chem. Phys. **149**, 210901 (2018).
[7] T. B. Schrøder and J. C. Dyre, J. Chem. Phys. **141**, 204502 (2014).
[8] P. A. Knudsen, "An investigation of isodynes in coarse grained ionic liquid models," Ph.D. thesis (Roskilde University, Denmark, 2022).
[9] P. A. Knudsen, D. M. Heyes, K. Niss, D. Dini, and N. P. Bailey, J. Chem. Phys. **160**, 034503 (2024).
[10] D. M. Heyes, D. Dini, S. Pieprzyk, and A. C. Brańka, J. Chem. Phys. **158**, 134502 (2023).
[11] D. M. Heyes, D. Dini, S. Pieprzyk, and A. C. Brańka, J. Chem. Phys. **159**, 224504 (2023).
[12] J.-P. Hansen, Phys. Rev. A **2**, 221 (1970).
[13] R. W. Zwanzig, J. Chem. Phys. **22**, 1420 (1954).
[14] S. A. Khrapak and A. G. Khrapak, Phys. Rev. E **103**, 042122 (2021).
[15] S. A. Khrapak, J. Chem. Phys. **156**, 116101 (2022).
[16] S. A. Khrapak and A. G. Khrapak, Phys. Fluids **34**, 027102 (2022).
[17] S. A. Khrapak and A. G. Khrapak, J. Phys. Chem. Lett. **13**, 2674 (2022).
[18] S. A. Khrapak and A. G. Khrapak, J. Chem. Phys. **157**, 014501 (2022).
[19] A. J. Schultz and D. A. Kofke, J. Chem. Phys. **149**, 204508 (2018).
[20] A. J. Schultz and D. A. Kofke, J. Chem. Phys. **153**, 059901 (2020).
[21] D. M. Heyes and A. C. Brańka, J. Chem. Phys. **143**, 234504 (2015).
[22] U. R. Pedersen, L. Costigliola, N. P. Bailey, T. B. Schrøder, and J. C. Dyre, Nat. Commun. **7**, 12386 (2016).
[23] L. Costigliola, T. B. Schrøder, and J. C. Dyre, Phys. Chem. Chem. Phys. **18**, 14678 (2016).
[24] M. Elenius and M. Dzugutov, J. Chem. Phys. **131**, 104502 (2009).
[25] Y. Rosenfeld, Chem. Phys. Lett. **38**, 591 (1976).
[26] Y. Rosenfeld, J. Chem. Phys. **63**, 2769 (1975).
[27] Y. Rosenfeld, Phys. Rev. E **62**, 7524 (2000).
[28] S. A. Khrapak, M. Chaudhuri, and G. E. Morfill, J. Chem. Phys. **134**, 094108 (2011).
[29] L. Bøhling, T. S. Ingebrigtsen, A. Grzybowski, M. Paluch, J. C. Dyre, and T. B. Schrøder, New J. Phys. **14**, 113035 (2012).
[30] N. P. Bailey, T. B. Schrøder, and J. C. Dyre, Phys. Rev. E **90**, 042310 (2014).
[31] S. Pieprzyk, A. C. Brańka, Sz. Maćkowiak, and D. M. Heyes, J. Chem. Phys. **148**, 114505 (2018).
[32] J. J. Nicolas, K. E. Gubbins, W. B. Streett, and D. J. Tildesley, Mol. Phys. **37**, 1429 (1979).
[33] D. M. Heyes, G. Rickayzen, S. Pieprzyk, and A. C. Brańka, J. Chem. Phys. **145**, 084505 (2016).
[34] M. P. Allen and D. J. Tildesley, *Computer Simulation of Liquids*, 2nd ed. (Oxford University Press, Oxford, 2017).
[35] D. M. Heyes, *The Liquid State: Applications of Molecular Simulations* (Wiley, Chichester, 1998).
[36] W. G. Hoover, Phys. Rev. A **31**, 1695 (1985).
[37] T. S. Ingebrigtsen, A. A. Veldhorst, T. B. Schrøder, and J. C. Dyre, J. Chem. Phys. **139**, 171101 (2013).
[38] A. Lofti, J. Vrabec, and J. Fischer, Mol. Phys. **76**, 1319 (1992).
[39] D. M. Heyes, S. Pieprzyk, and A. C. Brańka, Comput. Methods Sci. Technol. **29**, 45 (2023).
[40] J. K. Johnson, J. A. Zollweg, and K. E. Gubbins, Mol. Phys. **78**, 591 (1993).
[41] B. Widom, J. Chem. Phys. **39**, 2808 (1963).
[42] J. G. Powles, W. A. B. Evans, and N. Quirke, Mol. Phys. **46**, 1347 (1982); **51**, 1511 (1984).

[43]D. M. Heyes, Chem. Phys. **82**, 285 (1983).
[44]B. Smit and D. Frenkel, J. Phys.: Condens. Matter **1**, 8659 (1989).
[45]M. A. van der Hoef, J. Chem. Phys. **113**, 8142 (2000).
[46]S. Prestipino, F. Saija, and P. V. Giaquinta, J. Chem. Phys. **123**, 144110 (2005).
[47]A. Mirzaeinia, F. Feyzi, and S. M. Hashemianzadeh, J. Chem. Phys. **147**, 214503 (2017).
[48]D. Dhabal, A. H. Nguyen, M. Singh, P. Khatua, V. Molinero, S. Bandyopadhyay, and C. Chakravarty, J. Chem. Phys. **143**, 164512 (2015).
[49]A. Baram and Y. Rosenfeld, J. Phys. C: Solid State Phys. **13**, L787 (1980).
[50]Y. Rosenfeld and A. Baram, J. Chem. Phys. **75**, 427 (1981).
[51]Y. Song and E. A. Mason, Phys. Rev. A **44**, 8400 (1991).
[52]D. M. Heyes, S. M. Clark, and A. C. Brańka, J. Chem. Phys. **131**, 204506 (2009).
[53]D. M. Heyes, M. Cass, J. G. Powles, and W. A. B. Evans, J. Phys. Chem. B **111**, 1455 (2007).
[54]E. Attia, J. C. Dyre, and U. R. Pedersen, J. Chem. Phys. **157**, 034502 (2022).
[55]K. Meier, "Computer simulation and interpretation of the transport coefficients of the Lennard-Jones model fluid," Ph.D. thesis, University of the Federal Armed Forces Hamburg, 2002.
[56]K. Meier, A. Laesecke, and S. Kabelac, J. Chem. Phys. **121**, 3671 (2004).
[57]R. L. Rowley and M. M. Painter, Int. J. Thermophys. **18**, 1109 (1997).
[58]D. M. Heyes, Phys. Rev. B **37**, 5677 (1988).
[59]G. Galliéro, C. Boned, and A. Baylaucq, Ind. Eng. Chem. Res. **44**, 6963 (2005).
[60]M. P. Lautenschlaeger and H. Hasse, Fluid Phase Equilib. **482**, 38 (2019).
[61]S. Hess and D. J. Evans, Phys. Rev. E **64**, 011207 (2001).
[62]S. Viscardy, J. Servantie, and P. Gaspard, J. Chem. Phys. **126**, 184513 (2007).
[63]S. Pieprzyk, A. C. Brańka, D. M. Heyes, and M. N. Bannerman, Phys. Chem. Chem. Phys. **22**, 8834 (2020).
[64]B. A. Younglove and H. J. M. Hanley, J. Phys. Chem. Ref. Data **15**, 1323 (1986).
[65]D. M. Heyes, Comput. Methods Sci. Technol. **21**, 169 (2015).
[66]S. Pieprzyk, M. N. Bannerman, A. C. Brańka, M. Chudak, and D. M. Heyes, Phys. Chem. Chem. Phys. **21**, 6886 (2019).
[67]Y. Rosenfeld, J. Phys.: Condens. Matter **11**, 5415 (1999).
[68]I. C. Yeh and G. Hummer, J. Phys. Chem. B **108**, 15873 (2004).
[69]S. A. Khrapak, J. Phys. Chem. B **128**, 287 (2024).
[70]L. Costigliola, D. M. Heyes, T. B. Schrøder, and J. C. Dyre, J. Chem. Phys. **150**, 021101 (2019).
[71]S. A. Khrapak and A. G. Khrapak, Phys. Rev. E **104**, 044110 (2021).
[72]V. I. Kalikmanov, *Statistical Physics of Fluids* (Springer, Berlin, 2001).
[73]S. A. Khrapak, Phys. Rep. **1050**, 1 (2024).
[74]I. H. Bell, G. Galliero, S. Delage-Santacreu, and L. Costigliola, J. Chem. Phys. **152**, 191102 (2020).
[75]I. H. Bell, R. Messerly, M. Thol, L. Costigliola, and J. C. Dyre, J. Phys. Chem. B **123**, 6345 (2019).
[76]N. H. March and M. P. Tosi, *Atomic Dynamics in Liquids* (MacMillan Press, London, 1976) Appendix 6.4.